

# UC San Diego

## UC San Diego Previously Published Works

### Title

Chemical Mutagenesis of an Emissive RNA Alphabet

### Permalink

<https://escholarship.org/uc/item/3x21x106>

### Journal

Journal of the American Chemical Society, 137(46)

### ISSN

0002-7863

### Authors

Rovira, Alexander R

Fin, Andrea

Tor, Yitzhak

### Publication Date

2015-11-25

### DOI

10.1021/jacs.5b10420

Peer reviewed



Published in final edited form as:

*J Am Chem Soc.* 2015 November 25; 137(46): 14602–14605. doi:10.1021/jacs.5b10420.

## Chemical Mutagenesis of an Emissive RNA Alphabet

Alexander R. Rovira, Andrea Fin, and Yitzhak Tor\*

Department of Chemistry and Biochemistry, University of California, San Diego, La Jolla, California 92093-0358, United States

### Abstract

An evolved fluorescent ribonucleoside alphabet comprising isomorphous purine (<sup>tz</sup>A, <sup>tz</sup>G) and pyrimidine (<sup>tz</sup>U, <sup>tz</sup>C) analogues, all derived from isothiazolo[4,3-*d*]pyrimidine as a common heterocyclic core, is described. Structural and biochemical analyses illustrate that the nucleosides, particularly the *C*-nucleosidic purine analogues, are faithful isomorphous and isofunctional surrogates of their natural counterparts and show improved features when compared to an RNA alphabet derived from thieno[3,4-*d*]-pyrimidine. The restoration of the nitrogen in a position equivalent to the purines' N7 leads to "isofunctional" behavior, as illustrated by the ability of adenosine deaminase to deaminate <sup>tz</sup>A as effectively as adenosine, the native substrate.

Fluorescent nucleoside analogues, which have been developed to address the nonemissive nature of the nucleobases found in DNA and RNA, have found great utility in biophysical analysis and discovery assays.<sup>1</sup> In addition to favorable photophysical features, a key element that dictates their utility and ultimate use is their structural similarity to the native counterparts. Characterized as their isomorphous nature, researchers have tried to maximize this trait by minimizing changes to the Watson–Crick (WC) pairing face while introducing fluorescence-enhancing electronic perturbations.<sup>2</sup> The impact of these alterations on the physical properties (e.g., tautomerization) and photophysics (excited state level and dynamics) are, however, frequently unpredictable and ultimately empirically assessed.

We have previously completed the first emissive RNA alphabet,<sup>3</sup> comprising pyrimidine and purine analogues, all fundamentally derived from thieno[3,4-*d*]-pyrimidine as a common heterocyclic nucleus (Figure 1). While highly emissive and valuable as illustrated by several applications,<sup>4</sup> a limitation of the previously reported thieno analogues is the lack of the basic nitrogen, corresponding to N7 in the purine skeleton (Figure 1).<sup>5</sup> As many biomolecular

\*Corresponding Author. ytor@ucsd.edu.

#### ASSOCIATED CONTENT

##### Supporting Information

The Supporting Information is available free of charge on the ACS Publications website at DOI: 10.1021/jacs.5b10420.

Synthetic details, photophysical data, enzymatic protocols and HPLC traces (PDF)

X-ray crystallographic data for <sup>tz</sup>G (CIF)

X-ray crystallographic data for <sup>tz</sup>C (CIF)

X-ray crystallographic data for <sup>tz</sup>U (CIF)

X-ray crystallographic data for <sup>tz</sup>A (CIF)

The authors declare no competing financial interest.

interactions of purine nucleosides and nucleotides rely on the basicity and coordinating ability of this position, we have sought to reinstall this functionality into a new isomorphous RNA alphabet, with higher structural and electronic similarity to the native purines. Herein we report the synthesis, photophysical analysis, and performance of a next generation alphabet based on an isothiazolo[4,3-*d*]pyrimidine core. This atomic mutagenesis reinstates the basic moiety at the native position yielding analogues that better mimic a purine (Figure 1). This chemically evolved isomorphous alphabet was found to not only have unique photophysical features but also to be highly “isofunctional”, illustrated by the ability of adenosine deaminase (ADA) to deaminate the adenosine analogue as effectively as adenosine, the native substrate.

While standard conditions provided the isothiazole uridine and cytidine analogues **tzU** and **tzC**, respectively,<sup>6</sup> common approaches to forming the carbon–carbon glycosidic bonds of the adenosine and guanosine analogues failed under a wide variety of conditions.<sup>7,8</sup> A less common approach was required to form the desired connectivity.<sup>9</sup> A strategy starting from a ribofuranose-derived precursor as opposed to late-stage glycosylation with the nucleobase and desired sugar was conceived. To construct the *C*-glycosylated isothiazole ring, a ribofuranose derivative substituted with a primary thiol **3** was synthesized (Scheme 1), starting from a known benzyl-protected precursor, which was subjected to Swern oxidation conditions to give **1**.<sup>10</sup> Treatment of **1** with diodomethane and methyllithium furnished the primary halide **2**,<sup>11</sup> which was reacted with potassium thioacetate and reduced to give the primary thiol **3** (Scheme 1).

Reactions of **3** with both ester and amide-substituted *N*-tosyl derivatives **4a** and **4b** furnished the cyclized **5a** and **5b**, respectively, in good yields (Scheme 2).<sup>12</sup> To set the stereocenter at the anomeric carbon, reduction of **5a** and **5b** with triethylsilane and BF<sub>3</sub>·OEt<sub>2</sub> was found to be the most effective, yielding key precursors **6a** and **6b**, respectively (Scheme 2).<sup>13</sup> Only one diastereomer was isolated and found to be the desired one (see below). With this key substrate in hand, the synthesis of the protected guanosine analogue **7** was accomplished using a mild two-step, one-pot reaction with an isothiocyanate precursor.<sup>14</sup> After cleavage of the carbamate, deprotection using 1,2-ethanedithiol and BF<sub>3</sub>·OEt<sub>2</sub> yielded the final nucleoside **tzG**.<sup>15,16</sup> Synthesis of the adenosine analogue was accomplished via initial construction of the inosine analogue **8** using triethyl orthoformate. This was subsequently converted to the thioamide **9** by treatment with P<sub>2</sub>S<sub>5</sub> in pyridine followed by methanolic ammonia to give the protected final product, which was then subjected to the same deprotection conditions to afford **tzA** (Scheme 2).

Crystal structure determination confirmed the proposed structure and anomeric configuration of the modified ribonucleosides (Figure 2 and Tables S1–S4). In the solid state, the purine analogues **tzA** and **tzG** showed an anti-orientation at the glycosidic linkages, while the pyrimidines **tzU** and **tzC** were found to be in the syn-orientation (Figure 2). Rewardingly, analysis of **tzG**'s crystal packing pattern shows pairing through both the WC and Hoogsteen faces, which is identical to the pattern seen for guanosine in the solid state (Figure 3).<sup>17</sup> This intermolecular hydrogen bonding arrangement, illustrating the restoration of a “functional” Hoogsteen face and “N7”, suggests that **tzG** is likely to share **G**'s H-bonding and tautomeric preferences.

The fundamental spectroscopic properties, the sensitivity toward environmental polarity, and the spectroscopically derived  $pK_a$  values of the modified nucleoside analogues are listed in Table 1. The ground-state absorption spectra in aqueous solution displayed bathochromic-shifted maxima compared to the corresponding native nucleosides ranging from 312 to 338 nm for  ${}^t\text{U}$  to  ${}^t\text{A}$ , respectively (Figure 4a). Visible emission maxima ranging from 392 nm (for  ${}^t\text{U}$ ) to 459 nm (for  ${}^t\text{G}$ ) were observed for all modified nucleosides upon excitation at their maxima. The emission quantum yield of the purine analogues, 0.25 for  ${}^t\text{G}$  and 0.05 for  ${}^t\text{A}$ , was higher than the pyrimidine analogues, with 0.01 for  ${}^t\text{U}$  and 0.05 for  ${}^t\text{C}$  in water.

The absorption spectra taken in dioxane showed batho and hypochromic shifts for  ${}^t\text{A}$ ,  ${}^t\text{C}$ , and  ${}^t\text{G}$  in comparison to the aqueous solutions, while no significant variations were observed for  ${}^t\text{U}$ . The emission intensity is sensibly lower in dioxane. The fluorescence maxima displayed a remarkable hypsochromic shift for  ${}^t\text{G}$  and  ${}^t\text{U}$ , a slight blue-shift for  ${}^t\text{A}$ , and a bathochromic shift for  ${}^t\text{C}$ . This suggests a charge-transfer character of their excited states (Figure S5). This is manifested for all nucleosides, albeit to different extents, in their responsiveness toward polarity changes, as seen by the linear correlations between the measured Stokes shifts and microscopic solvent polarity parameters (Figure 4b, Table 1).

All new nucleosides display sensitivity toward pH variations, thus facilitating the extraction of  $pK_a$  values (Figure 4c,d and Table 1). The deprotonation of  ${}^t\text{U}$  between pH 8 and 11 is characterized by a red shift of its absorption maximum yielding a  $pK_a$  value of 8.9, which is comparable to the values reported for N3 deprotonation in uridine ( $pK_a$  9.20–9.25).<sup>18</sup>  ${}^t\text{C}$  is the least responsive to pH changes, displaying minor blue shifts in both the absorption and emission spectra (Figure 4c,d), and yielding two  $pK_a$  values (Table 1).  ${}^t\text{A}$  was characterized by a bathochromic shift both in its absorption and emission maxima upon deprotonation of N1 ( $pK_a = 4.25$  and  $3.29$ , respectively) in close proximity to the reported values for adenosine ( $pK_a$  3.6–4.2).<sup>19</sup> pH titration of  ${}^t\text{G}$  showed two distinct red-shifted transitions of the absorption maximum and two different isosbestic points at 325 and 333 nm (Figure S2), assigned to deprotonation of N7 and N1 ( $pK_a = 3.55$  and  $8.51$ , respectively). These values correlate well with the reported values for guanosine ( $pK_a = 3.2$ – $3.3$  and  $9.2$ – $9.6$ , respectively).<sup>20</sup> Taken together, these observations not only illustrate the responsiveness of these nucleosides, but further indicate the ability of the isothiazole ring to mimic the basic imidazole moiety in the native purines.

To demonstrate the utility of the new analogues and the impact of restoring the basic N7 in evolving the thieno alphabet into the isothiazolo one, we selected to probe the enzymatic deamination of adenosine to inosine. This important metabolic transformation is catalyzed by adenosine deaminase (ADA).<sup>21</sup> We have previously reported the ability of ADA to recognize and deaminate  ${}^{th}\text{A}$ , the thieno[3,4-*d*]-pyrimidine-based analogue of the naturally occurring adenosine, to  ${}^{th}\text{I}$  (Figure 5a), the corresponding inosine derivative. While of significance in and of itself, the enzymatic conversion of  ${}^{th}\text{A}$  to  ${}^{th}\text{I}$  was, however, approximately 20-times slower compared to that of adenosine.<sup>4b</sup> Since ADA has been crystallographically shown to form a H-bond to the N7 of its substrate,<sup>21a,b</sup> we hypothesized that restoration of this functionality in  ${}^t\text{A}$ , the new adenosine surrogate, should facilitate its deamination compared to  ${}^{th}\text{A}$ .

Steady state absorption and emission spectra, taken at defined time-intervals upon addition of ADA to **tzA**, showed a fast and efficient conversion of **tzA** to **tzI** (Figure S6). Real-time continuous measurements, relying on the photophysical differences between **tzA** and **tzI**, **thA** and **thI**, and **A** and **I**,<sup>4b,22</sup> show that, while the deamination reaction of **thA** is indeed sluggish, ADA deaminates **tzA** to **tzI** at the same rate as it deaminates **A** to **I** (Figure 5b). The reaction half-life for **tzA** deamination, calculated assuming a pseudo-first order reaction, was comparable to the one observed for adenosine, the native substrate ( $t_{1/2} = 39$  and  $57$  s, respectively) and substantially shorter than the one obtained for **thA** ( $t_{1/2} = 818$  s). This remarkable initial deamination rate of **tzA** by ADA, substantiating our hypothesis, was confirmed by HPLC analyses (Figure 5c inset, Figure S8). Taken together, these observations highlight the improved functionality of the isothiazolopyrimidine over the thienopyrimidine core.

In summary, we introduce a second-generation family of emissive nucleoside analogues, based on an isothiazolopyrimidine scaffold. This atomic mutation results in higher isomorphism and significantly improved functionality when compared to the thienopyrimidine-based RNA alphabet. The presence of the isothiazole core with its nitrogen in the equivalent position to N7 of the native purines, restores the Hoogsteen face, as well as the basicity and native H bonding ability of these surrogates, as illustrated structurally (for **tzG**) and biochemically (for **tzA** deamination by ADA). These observations, indicating that the newly introduced purine surrogates display improved structural and functional characteristics, are of significance since very few emissive, isomorphous, and non-perturbing purine analogues have so far been made and biophysically exploited.

## Supplementary Material

Refer to Web version on PubMed Central for supplementary material.

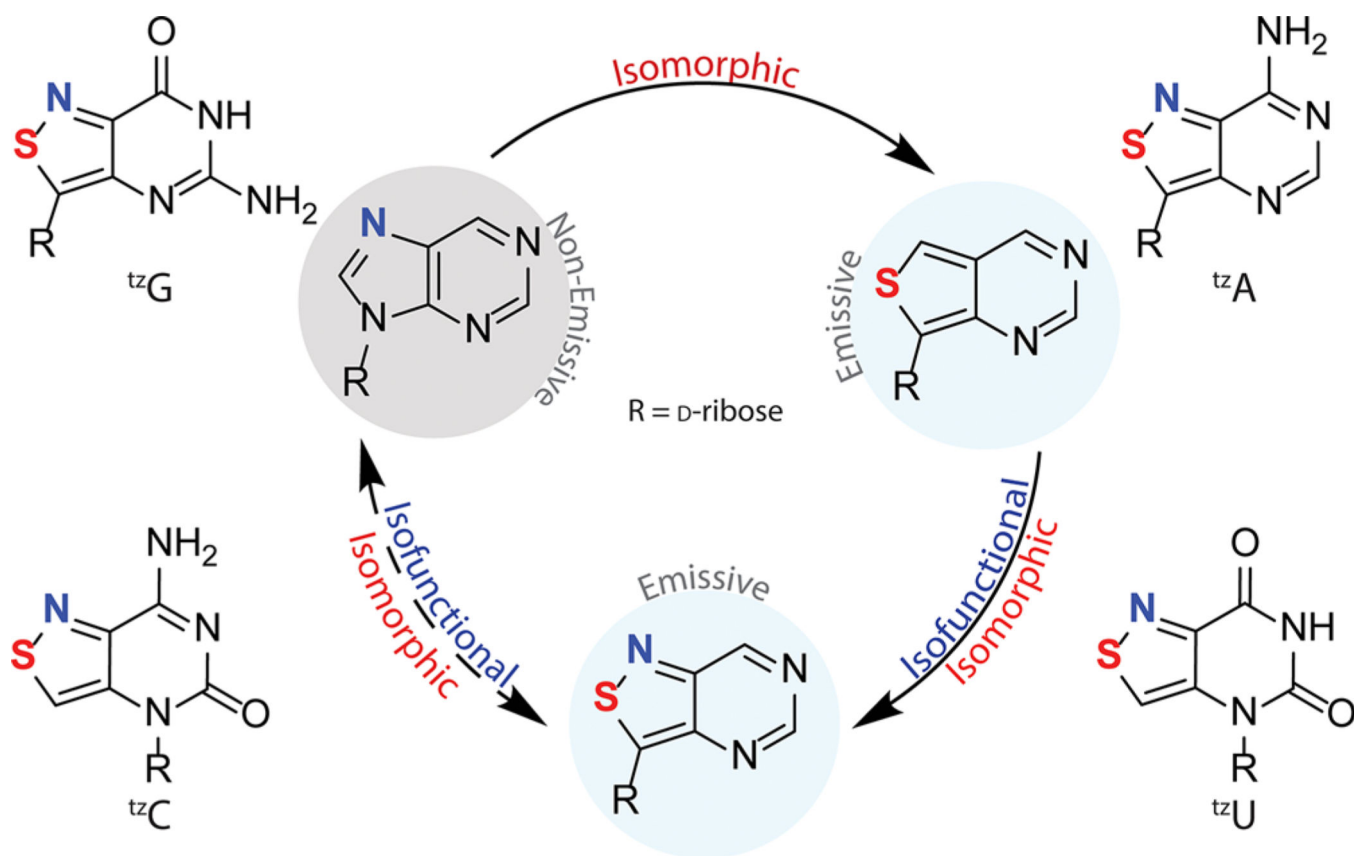
## Acknowledgments

We thank the National Institutes of Health for generous support (GM 069773), the Chemistry and Biochemistry MS Facility, and the UCSD X-ray crystallography Facility.

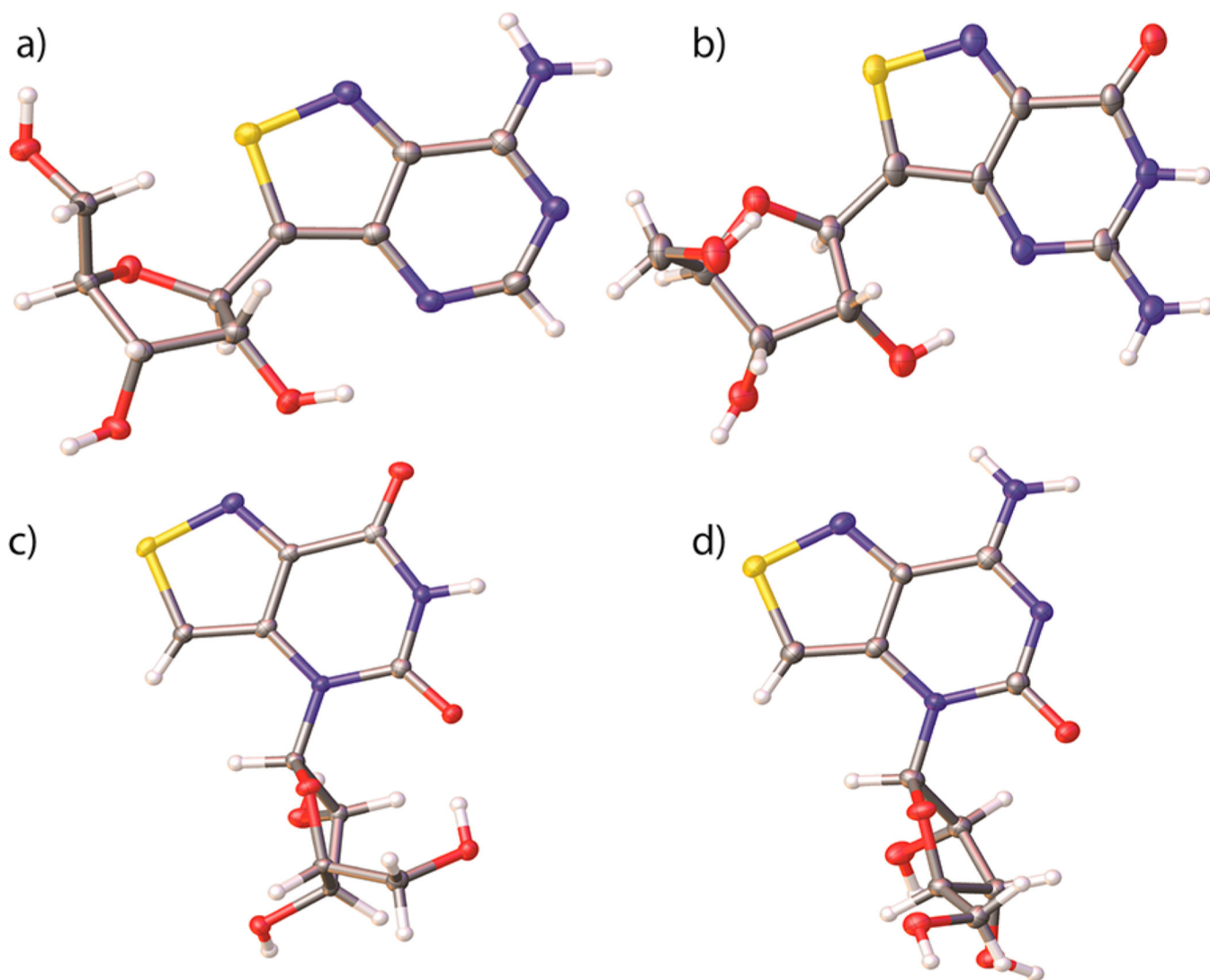
## REFERENCES

- (a) Sinkeldam RW, Greco NJ, Tor Y. *Chem. Rev.* 2010; 110:2579–2619. [PubMed: 20205430] (b) Wilhelmsson MQ. *Rev. Biophys.* 2010; 43:159–183. (c) Hawkins ME. *Cell Biochem. Biophys.* 2001; 34:257–281. [PubMed: 11898867] (d) Wilson JN, Kool ET. *Org. Biomol. Chem.* 2006; 4:4265–4274. [PubMed: 17102869] (e) Okamoto A, Saito Y, Saito I. *J. Photochem. Photobiol., C.* 2005; 6:108–122. (f) Dodd DW, Hudson RHE. *Mini-Rev. Org. Chem.* 2009; 6:378–391. (g) Kimoto M, Cox RS III, Hirao I. *Expert Rev. Mol. Diagn.* 2011; 11:321–331. [PubMed: 21463241] (h) Rist MJ, Marino JP. *Curr. Org. Chem.* 2002; 6:775–793. (i) Wierzchowski J, Antosiewicz JM, Shugar D. *Mol. BioSyst.* 2014; 10:2756–2774. [PubMed: 25124808]
- (a) Gaied NB, Glasser N, Ramalanjaona N, Beltz H, Wolff P, Marquet R, Burger A, Mely Y. *Nucleic Acids Res.* 2005; 33:1031–1039. [PubMed: 15718302] (b) Nadler A, Strohmeier J, Diederichsen U. *Angew. Chem., Int. Ed.* 2011; 50:5392–5396. (c) Dierckx A, Miannay F-A, Gaied NB, Preus S, Björck M, Brown T, Wilhelmsson LM. *Chem. - Eur. J.* 2012; 18:5987–5997. [PubMed: 22437923] (d) Dumat B, Bood M, Wranne MS, Lawson CP, Foller Larsen A, Preus S, Streling J, Gradén H, Wellner E, Grøtli M, Wilhelmsson LM. *Chem. - Eur. J.* 2015; 21:4039–4048. [PubMed: 25641628] (e) Greco NJ, Tor Y. *J. Am. Chem. Soc.* 2005; 127:10784–10785. [PubMed: 16076156]

3. Shin D, Sinkeldam RW, Tor Y. *J. Am. Chem. Soc.* 2011; 133:14912–14915. [PubMed: 21866967]
4. (a) Liu W, Shin D, Tor Y, Cooperman BS. *ACS Chem. Biol.* 2013; 8:2017–2023. [PubMed: 23865809] (b) Sinkeldam RW, McCoy LS, Shin D, Tor Y. *Angew. Chem., Int. Ed.* 2013; 52:14026–14030. (c) McCoy LS, Shin D, Tor Y. *J. Am. Chem. Soc.* 2014; 136:15176–15184. [PubMed: 25255464] (d) Otomo H, Park S, Yamamoto S, Sugiyama H. *RSC Adv.* 2014; 4:31341–31344. (e) Park S, Otomo H, Zheng L, Sugiyama H. *Chem. Commun.* 2014; 50:1573–1575. (f) Sholokh M, Sharma R, Shin D, Das R, Zaporozhets OA, Tor Y, Mely Y. *J. Am. Chem. Soc.* 2015; 137:3185–3188. [PubMed: 25714036]
5. Mizrahi RA, Shin D, Sinkeldam RW, Phelps KJ, Fin A, Tantillo DJ, Tor Y, Beal PA. *Angew. Chem., Int. Ed.* 2015; 54:8713–8716.
6. The synthesis of the pyrimidine analogues is described in the Supporting Information (Scheme S5).
7. (a) Coté, GL., Flitsch, S., Ito, Y., Kondo, H., Nishimura, S., Yu, B., Fraser-Reid, BO., Tatsuta, K., Thiem, J. *Glycoscience: Chemistry and Chemical Biology*. 2. Berlin Heidelberg: Springer-Verlag; 2008. (b) Iddon B. *Heterocycles*. 1995; 41:533–593. (c) Stambasky J, Hocek M, Kocovsky P. *Chem. Rev.* 2009; 109:6729–6764. [PubMed: 19761208]
8. Attempts to glycosylate the nucleobase using palladium coupling chemistry, grignard formation, alkylolithium chemistry, and standard Vorgbruggen glycosylation conditions were all unsuccessful.
9. Wamhoff H, Berressem R, Nieger M. *J. Org. Chem.* 1993; 58:5181–5185.
10. See Supporting Information (Scheme S1).
11. Bessieres B, Morin C. *Synlett*. 2000:1691–1693.
12. Gewald K, Bellmann P. *Liebigs Ann. Chem.* 1979; 1979:1534–1546.
13. van Rijssel ER, van Delft P, Lodder G, Overkleeft HS, van der Marel GA, Filippov DV, Codée JDC. *Angew. Chem., Int. Ed.* 2014; 53:10381–10385.
14. Lecoutey C, Fossey C, Rault S, Fabis F. *Eur. J. Org. Chem.* 2011; 2011:2785–2788.
15. Fuji K, Ichikawa K, Node M, Fujita E. *J. Org. Chem.* 1979; 44:1661–1664.
16. Seley KL, Zhang L, Hagos A, Quirk S. *J. Org. Chem.* 2002; 67:3365–3373. [PubMed: 12003548]
17. (a) Additionally, an overlay of the purine analogues and natural nucleosides may be found on Figure S1. Marsh RE, Bugg CE, Thewalt U. *Acta Crystallogr., Sect. B: Struct. Crystallogr. Cryst. Chem.* 1970; B26:1089–1101.
18. (a) Simpson RB. *J. Am. Chem. Soc.* 1964; 86:2059–2065. (b) Luyten I, Pankiewicz KW, Watanabe KA, Chattopadhyaya J. *J. Org. Chem.* 1998; 63:1033–1040.
19. (a) Christensen JJ, Rytting JH, Izatt RM. *Biochemistry*. 1970; 9:4907–4913. [PubMed: 5480155] (b) Kapinos LE, Operschall BP, Larsen E, Sigel H. *Chem. - Eur. J.* 2011; 17:8156–8164. [PubMed: 21626581]
20. (a) Bundari, S. *The Merck Index*. 12th. Whitehouse Station, NJ: Merck and Co., Inc; 1996. (b) Sigel H, Massoud SS, Corfù NA. *J. Am. Chem. Soc.* 1994; 116:2958–2971. (c) Thapa B, Schlegel HB. *J. Phys. Chem. A*. 2015; 119:5134–5144. [PubMed: 25291241] (d) Kampf G, Kapinos LE, Griesser R, Lippert B, Sigel H. *J. Chem. Soc., Perkin Trans.* 2002; 2:1320–1327.
21. (a) Kinoshita T, Nishio N, Nakanishi I, Sato A, Fujii T. *Acta Crystallogr., Sect. D: Biol. Crystallogr.* 2003; 59:299–303. [PubMed: 12554940] (b) Wilson DK, Rudolph FB, Quiocho FA. *Science*. 1991; 252:1278–1284. [PubMed: 1925539] (c) Kinoshita T, Nakanishi I, Terasaka T, Kuno M, Seki N, Warizaya M, Matsumura H, Inoue T, Takano K, Adachi H, Mori Y, Fujii T. *Biochemistry*. 2005; 44:10562–10569. [PubMed: 16060665]
22. See Supporting Information (Figure S6).

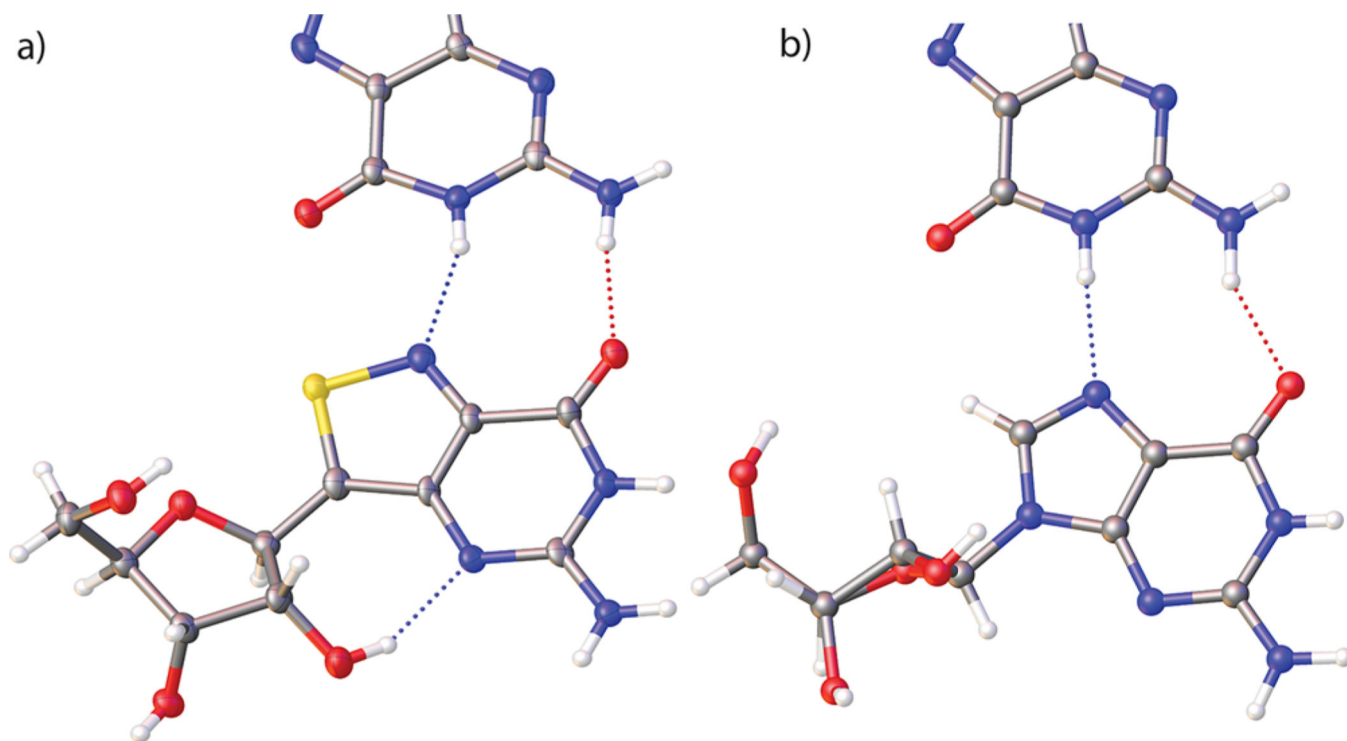


**Figure 1.**  
Evolution of an emissive RNA alphabet.

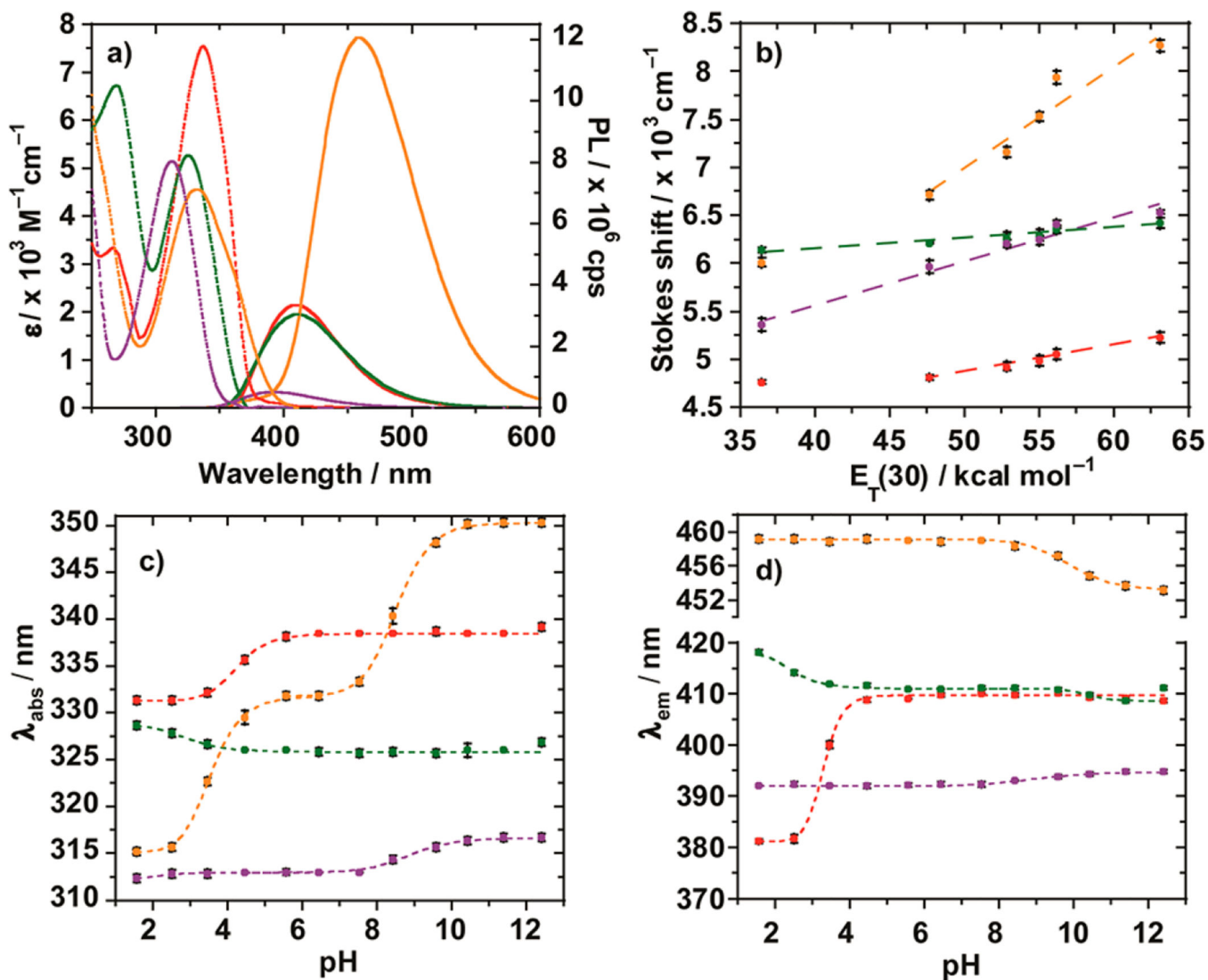


**Figure 2.** X-ray crystal structures of isothiazolo[4,3-*d*]pyrimidine analogues: (a) <sup>tz</sup>A, (b) <sup>tz</sup>G, (c) <sup>tz</sup>U, and (d) <sup>tz</sup>C.



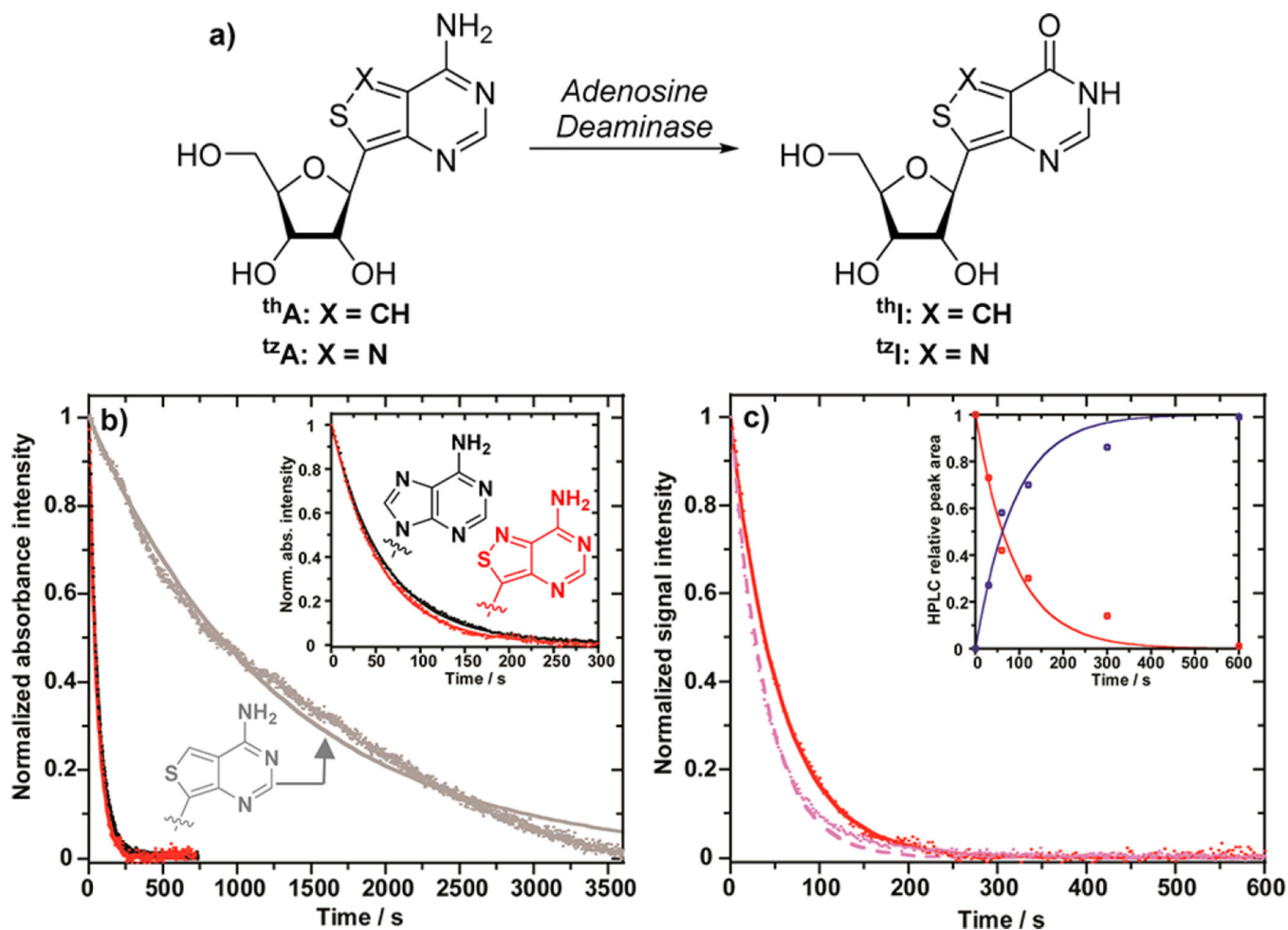


**Figure 3.**  
Comparison of intermolecular H-bonding seen in the crystal structures of (a)  $tG$  and (b)  $G$ .



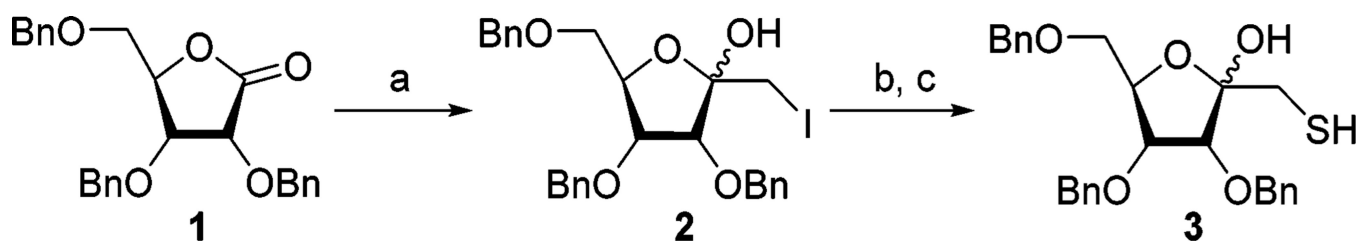
**Figure 4.**

(a) Absorption (dashed lines) and emission (solid lines) spectra of **tZA** (red), **tZC** (green), **tZG** (orange), and **tZU** (purple) in water. (b) Stokes shift correlation versus solvent polarity ( $E_T(30)$ ) of water/dioxane mixtures for **tZA** (red), **tZC** (green), **tZG** (orange), and **tZU** (purple). (c) Absorption maxima and (d) emission maxima variation versus pH for **tZA** (red), **tZC** (green), **tZG** (orange), and **tZU** (purple).

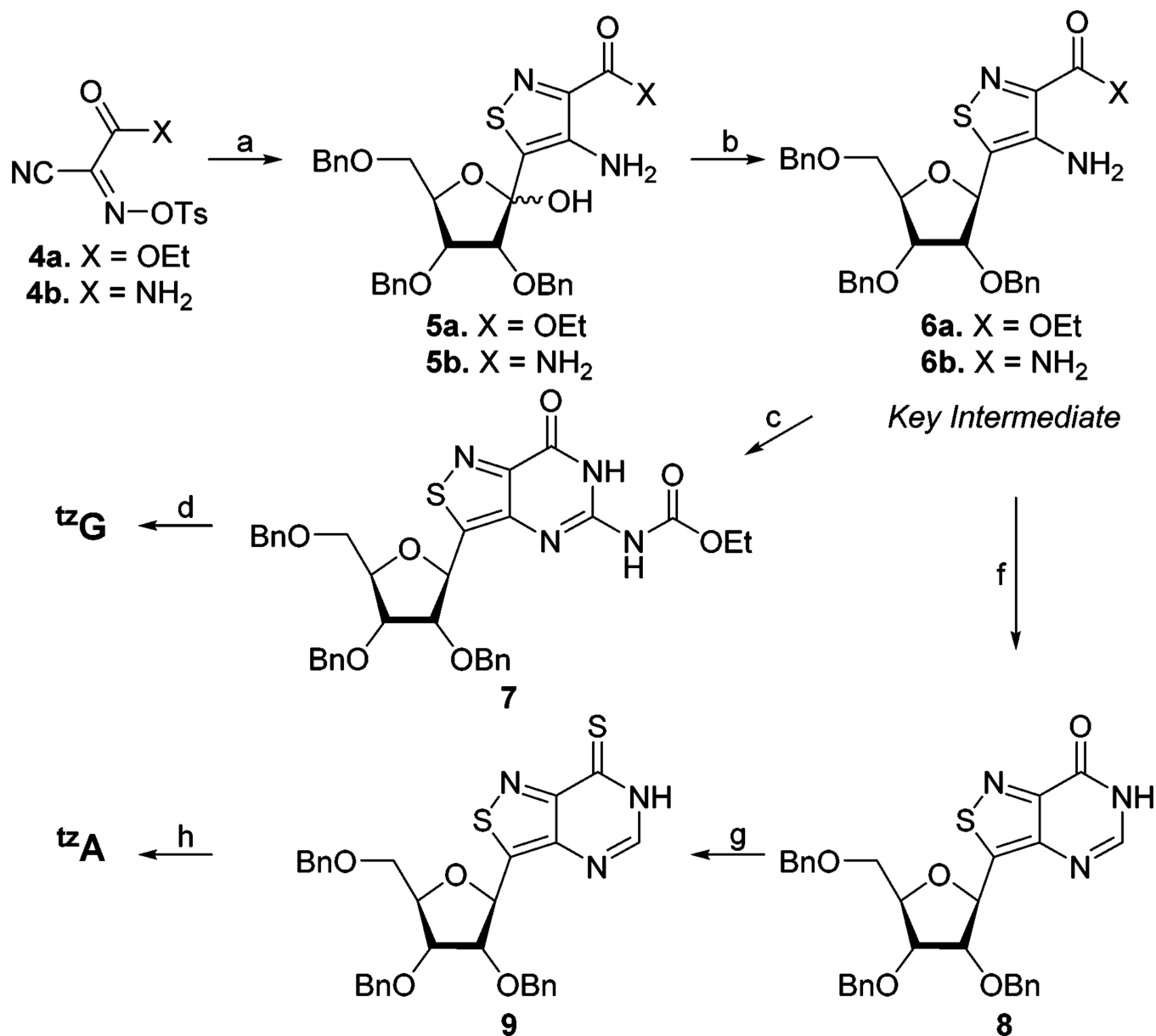


**Figure 5.**

(a) Deamination of **thA** and **tzA**. (b) Enzymatic deamination of **A** to **I** (black), **tzA** to **tzI** (red), and **thA** to **thI** (gray) with ADA monitored by real-time absorption at 260, 340, and 340 nm, respectively. Inset: zoomed in region between 0 and 300 s. (c) Enzymatic deamination of **tzA** to **tzI** by ADA monitored by real-time absorption (red) at 340 nm and real time emission (light purple) at 410 nm (excitation at 322 nm). Inset: HPLC relative peak area variation at different time-points for **tzA** (red) and **tzI** (blue) monitored at 340 nm.

**Scheme 1. Synthesis of the Sugar Precursor<sup>a</sup>**

<sup>a</sup>Reagents and conditions: (a)  $\text{CH}_2\text{I}_2$ , MeLi, toluene,  $-78\text{ }^\circ\text{C}$ , 1 h, 67%. (b) Potassium thioacetate, DMF, rt, 6 h, 74%. (c)  $\text{Et}_2\text{O}$ ,  $\text{LiAlH}_4$ ,  $0\text{ }^\circ\text{C}$  to rt, 1 h, >90%.



### Scheme 2. Synthesis of Purine Analogues

<sup>a</sup>Reagents and conditions: (a) **3**, EtOH, morpholine, 5 h, 0 °C to rt, 67% (**5a**), 79% (**5b**). (b) Et<sub>3</sub>SiH, BF<sub>3</sub>·OEt<sub>2</sub>, DCM, -78 °C to rt, 4 h, 63% (**6a**), 79% (**6b**). (c) i. EtOC(O)NCS, CH<sub>3</sub>CN, rt, 4 h; ii. EDCl, HMDS, rt, 48 h, 63% (d) i. 1 M NaOH, MeOH, 65 °C; ii. HSCH<sub>2</sub>CH<sub>2</sub>SH, BF<sub>3</sub>·OEt<sub>2</sub>, DCM, rt, 48 h, 59%. (f) CH(OEt)<sub>3</sub>, Ac<sub>2</sub>O, 120 °C, 16 h, 69%. (g) P<sub>2</sub>S<sub>5</sub>, pyridine, 65 °C, 2 h. (h) i. NH<sub>3</sub>, MeOH, 70 °C, 16 h; ii. HSCH<sub>2</sub>CH<sub>2</sub>SH, BF<sub>3</sub>·OEt<sub>2</sub>, DCM, rt, 72 h, 32% (for steps g and h).

Table 1

Photophysical Properties of Isothiazolo[4,3-*d*]pyrimidine Nucleoside Analogues

	solvent	$\lambda_{\text{abs}}$ (e) <sup>a</sup>	$\lambda_{\text{em}}$ (e) <sup>a</sup>	$\Phi_e$	Stokes shift <sup>a</sup>	polarity sensitivity <sup>b</sup>	p <i>K</i> <sub>a</sub> <sup>c</sup>	
							abs	em
<b>trA</b>	water	338 (7.79)	410 (0.05)	413	5.23	27.7	4.25	3.29
	dioxane	342 (7.42)	409 (0.03)	193	4.76			
<b>trC</b>	water	325 (5.45)	411 (0.05)	289	6.42	10.5	2.94	2.46, 10.38
	dioxane	333 (5.03)	419 (0.04)	181	6.14			
<b>trG</b>	water	333 (4.87)	459 (0.25)	1203	8.27	102.0	3.55, 8.51	9.88
	dioxane	339 (4.65)	425 (0.17)	539	6.01			
<b>trU</b>	water	312 (5.17)	392 (0.01)	41	6.53	45.4	2.25, 8.88	8.94
	dioxane	314 (5.20)	377 (<0.01)	21	5.36			
<b>trI</b>	water	316 (7.63)	377 (0.01)	46	5.13	12.7	9.26	7.83
	dioxane	315 (6.62)	372 (<0.01)	26	4.79			

<sup>a</sup>  $\lambda_{\text{abs}}$ , e,  $\lambda_{\text{em}}$ , and Stokes shift are reported in nm,  $10^3 \text{ M}^{-1} \text{ cm}^{-1}$ , nm, and  $10^3 \text{ cm}^{-1}$ , respectively. All photophysical values reflect the average of at least three independent measurements.

<sup>b</sup> Sensitivity to solvent polarity reported in  $\text{cm}^{-1}/(\text{kcal mol}^{-1})$  is equal to the slope of the linear fit in Figure 4b.

<sup>c</sup> p*K*<sub>a</sub> values reflect the average over three independent measurements and are equal to the inflection point determined by the fitting curves in Figure 4c,d. See Supporting Table S5 for expanded data including experimental errors.